Effective Gouge-Free Tool Selection for Free-Form Surface Machining

Daoshan OuYang[1], Hsi-Yung Feng[2], Benjamin A. Van Nest[3] and Ralph O. Buchal[4]

[1]Husky Injection Molding Systems Ltd., daoshan.ouyang@gmail.com
[2]The University of British Columbia, feng@mech.ubc.ca
[3]Deltaplast Machinery Ltd., bvannest@deltaplastmachinery.com
[4]The University of Western Ontario, rbuchal@eng.uwo.ca

ABSTRACT

This paper presents an efficient method to reliably approximate medial axis spheres for free-form surfaces. The calculated results are directly applicable to the selection of gouge-free ball-end mills in three-axis free-form surface machining. The medial axis sphere at each point on the surface is a global geometric property and equivalent to the maximum non-gouging ball-end mill size at the point. The fundamental concept is that the union of a point's incident Delaunay spheres encompasses all spheres that pass through the point and contain no other point inside. This leads to the present method of approximating the medial axis sphere at a point via considering only its Voronoi neighbors on the machining side of its tangent plane. The approximation accuracy can be further improved by considering additionally sampled points around the Voronoi neighbors. Extensive case studies have been carried out to demonstrate the effectiveness of the present method in selecting gouge-free cutting tools.

Keywords: tool selection, machining, gouging, medial axis sphere, free-form surface.
DOI: 10.3722/cadaps.2009.839-849

1. INTRODUCTION

Objects with free-form surfaces are common in practice such as ship hulls, propellers, automobile body panels, aircraft fairing surfaces, and aerospace engine parts. With today's computers and shape scanning devices becoming more and more sophisticated, representing the geometry of these objects using the point cloud based format is now a viable option. Generally, an object is represented by points because it contains unknown free-form surface geometry. Nonetheless, even when the exact mathematical representation of the surface is known, it is becoming a general practice to employ a triangular mesh to approximate the free-form surface to generate the NC tool path. The vertices of the triangular mesh are sometimes also viewed as a point cloud representation of the free-form surface.

For point cloud based surface representations, various methods have been proposed to generate NC tool paths directly from the discrete coordinate points [5],[9],[13],[16],[17]. However, comparatively less work has been done on tool selection. For both roughing and finishing machining operations, it is essential to determine the largest tool size that is able to carry out the intended machining operation without gouging. The direct benefit of using the largest-sized tool is reduced scallop size, in particular for three-axis machining with a ball-end mill. More importantly, larger tools are more rigid and able to carry out the machining operation with much increased feed rate. Most existing methods, such as [11],[12],[21],[22], analyze geometric features in smooth and continuous surfaces to select the gouge-free cutter or cutters. Only recently, the point cloud based surface representations were employed to

resolve the tool selection problem. One such method is based on the concept of Delaunay pole spheres, developed by researchers in computer graphics and visualization [1]. The Delaunay poles spheres are the two unique largest empty spheres respectively on each side of the surface at a given point. The smallest Delaunay pole sphere size on the machining side of the surface could then be regarded as the optimal ball-end mill size [15] for three-axis free-form surface machining. Since the points are only a sample of the surface, estimated normal vectors [14] were to be employed to improve the calculation accuracy.

Research studies dealing with free-form surface machining, e.g. [11], have been determining tool size for the finishing machining operation using surface curvatures. It should be noted that curvature is a local geometric property and only suitable for local gouging avoidance at (or in the immediate vicinity of) the cutter contact point on the surface. Curvature contains no geometric information of the surface away from the cutter contact point and thus cannot be used to detect global gouging at the ball part of the ball-end mill. In fact, in three-axis free-form surface machining without the concern of interference at the tool shank, global gouging is the primary concern for most tool accessibility issues. Because of this, the medial axis sphere at each point, which is a global property of the surface, is to be used for determining the optimal ball-end mills in machining the free-form surfaces.

2. MEDIAL AXIS
The medial axis of a surface in three dimensions is defined as the locus of points that have two or more (generally two) closest points on the surface. Each point $\mathbf{C}$ on the medial axis can be considered as the center of a maximized empty sphere (medial axis sphere) that does not contain any part of the surface within its interior and touches at least two points, $\mathbf{P}_i$ ($i = 1 \ldots k, k \geq 2$), on the surface. $\mathbf{C}$ is in the surface normal direction of $\mathbf{P}_i$. The medial axis can also be formulated as the locus of the center of a maximal deformable sphere as it rolls around the surface. It is thus evident that the medial axis sphere is the theoretical solution for the optimal tool size at the corresponding point.

Medial axis was first introduced by Blum [3] for the analysis of biological shapes. Since then, it has been widely used in many two-dimensional applications, such as image processing, path planning, finite element mesh generation, and feature recognition. Medial axis can also be used to analyze 3D shapes [4]. Some researchers have used it as a representation of deformable objects [18]. Extensive research has been carried out to analyze two-dimensional medial axis. For example, Culver et al. [6] have introduced algorithms for computing exact medial axis in three dimensions for some simple shapes such as polyhedra. However, it is in fact difficult to construct the exact medial axis for general surface shapes in three dimensions. Thus, continued efforts have been made to approximate the medial axis for three-dimensional applications.

Many researchers have been using sampled points from a given surface and approximating the medial axis via the Voronoi diagram of these points. Typically, these researchers used all of the Voronoi vertices to approximate the medial axis under the assumption that the Voronoi vertices would converge to the theoretical medial axis with increasing point sampling density [2],[19],[20]. Amenta et al. [1] have proved that the Voronoi pole vertices do converge to the medial axis and proposed to use the union of every point's pole spheres to approximate the sampled object geometry and to use the medial axis of the union spheres to approximate the exact medial axis. Dey and Zhao [8] proposed to use user-defined angle and length criteria to select Voronoi facets directly from the Voronoi diagram to approximate the medial axis. This is based on the observation that each point's Voronoi cell will be elongated along the point's normal direction as the point density increases.

This paper proposes a new method that can efficiently and reliably approximate the medal axis sphere for each point in a set of sampled points. The medial axis sphere center of a point $\mathbf{P}$ is to be on its surface normal and the sphere will touch at least one other sampled point $\mathbf{Q}$ and contain no other sampled point inside. Thus a medial axis sphere center will be on the Voronoi cell boundary of $\mathbf{P}$ but is not necessarily a Voronoi cell vertex. It is evident that $\mathbf{Q}$ is a Voronoi neighbor of $\mathbf{P}$. The medial axis sphere at $\mathbf{P}$ can then be approximated from its surface normal and Voronoi neighbors, as to be

described in the next section. If the surface normal vectors of the sampled points are not readily available, the method by OuYang and Feng [14] can be employed to estimate the normal vectors at the sampled points due to its demonstrated consistency under varying geometric complexity and sampled point density. A specific algorithm is devised to further improve the accuracy of the approximated medial axis sphere for the sampled points when the underlying sampled surface is unknown.

3. MEDIAL AXIS SPHERE APPROXIMATION

As stated in the previous section, a medial axis sphere at a point on a surface represents the largest sphere that touches the surface at the given point and at least one other point without having any other part of the surface contained within it. A point's medial axis sphere center has to be on the point's surface normal. It was proposed to approximate the medial axis sphere at a given point $\mathbf{P}$ by creating an initial sphere with the sphere center on the point's normal using an arbitrarily large and exaggerated radius. The center of the initial sphere was then updated along the surface normal using a point found to be closer to the initial sphere center than $\mathbf{P}$. This was an iterative process that needed to examine every point on the surface. The point that constrains the smallest sphere is defined as the gouging point of $\mathbf{P}$. The computational complexity of this algorithm is $\mathbf{O}(n^2)$, where n is the number of the sampled points.

It can be shown, and as one would expect, that the sampled point density of the surface plays a vital role in the accuracy of the calculated medial axis sphere size. It would seem that the accuracy issue could be easily resolved by sampling a very large point set from the surfaces however, there is the potential of incurring a major computing time penalty in doing so. The computer resources necessary to process massive data point sets, along with the computing time required for the related tasks, is sometimes a price too high to pay for the improvements that may be gained. In order to realize the improvements that come by increasing the point density of a known geometric surface representation, and not have to suffer the consequences therein, an improved and more computationally efficient algorithm would have to be developed.

In order to maximize the efficiency of the search algorithm, the number of unnecessary points that need to be visited must be reduced as much as possible. A point is deemed unnecessary if it has no limiting effect on the medial axis sphere size at the given point. It would be difficult, however, to recognize these points without calculating the distances between them and the others. The Voronoi diagram of the sampled point set will provide this relationship efficiently for all the sampled points.

In this work, the Voronoi diagram is generated using the publicly available C++ library called CGAL [10], which is known to be accurate and efficient. It is well established that the Voronoi diagram of n points (or sites) will divide the space into n Voronoi cells. Each site corresponds to one Voronoi cell such that any point inside this cell is closer to this site than to any other sites. Delaunay triangulation is the dual of Voronoi diagram. The space, instead of being partitioned into Voronoi cells, is now partitioned into Delaunay simplex, for example, Delaunay triangles in the 2D space and Delaunay tetrahedrons in the 3D space. In the 2D space, each Delaunay triangle connects three sites and its circumcircle will contain no site inside. In this work, each circumcircle of a Delaunay triangle is referred to as a Delaunay circle. In the 3D space, the circumsphere of a Delaunay tetrahedron, which connects four sites, is referred to as a Delaunay sphere.

Fig. 1 shows the basic elements of a 2D Voronoi diagram and Delaunay triangulation pertaining to a sampled point $\mathbf{S}_0$. In this figure, sampled points $\mathbf{S}_i$ ($i = 1...5$) are the Voronoi neighbors of $\mathbf{S}_0$. Each vertex $\mathbf{P}_i$ ($i = 1...5$) of the Voronoi cell of $\mathbf{S}_0$ is the Delaunay circle center. For example, $\mathbf{P}_1$ is the Delaunay circle center of the Delaunay triangle $\mathbf{S}_0 \mathbf{S}_1 \mathbf{S}_5$. It is evident that the union of the Delaunay circles at $\mathbf{S}_0$ will include all circles that pass through $\mathbf{S}_0$ and contain no sampled point inside. In other words, if any 2D circle, containing no sampled point inside, touches $\mathbf{S}_0$ and another sampled point $\mathbf{S}$, then $\mathbf{S}$ must be a Voronoi neighbor of $\mathbf{S}_0$ and its center $\mathbf{C}$ has to be on the Voronoi cell boundary. It

is because $\mathbf{C}$ cannot be inside of the Voronoi cell of $\mathbf{S}_0$; otherwise it contradicts the Voronoi cell definition that requires any point in the Voronoi cell is closer to $\mathbf{S}_0$ than to any other point. $\mathbf{C}$ cannot be outside of the Voronoi cell; otherwise $\mathbf{C}$ is closer to another site and the circle will then include such a site inside. Thus $\mathbf{C}$ has to be on the Voronoi cell boundary. And according to the Voronoi cell definition, $\mathbf{S}$ must be one of the Voronoi neighbors of $\mathbf{S}_0$. The same conclusion can also be extended to higher dimensional space. For example, in the 3D space, if any sphere contains no sampled point inside and passes through two sampled points $\mathbf{S}_i$ and $\mathbf{S}_j$, then $\mathbf{S}_i$ and $\mathbf{S}_j$ must be Voronoi neighbors.

It is thus unnecessary to examine every sampled point to approximate the medial axis sphere at a given point. Only the Voronoi neighbors on the machining side of the point's tangent plane need to be checked. For example, in Fig. 1, only $\mathbf{S}_1$ and $\mathbf{S}_5$ are checked to approximate the medial axis sphere at $\mathbf{S}_0$ due to the indicated normal direction. Also, in order to improve the accuracy of the approximated medial axis sphere, more points can be sampled and checked in the vicinity of $\mathbf{S}_1$ and $\mathbf{S}_5$.
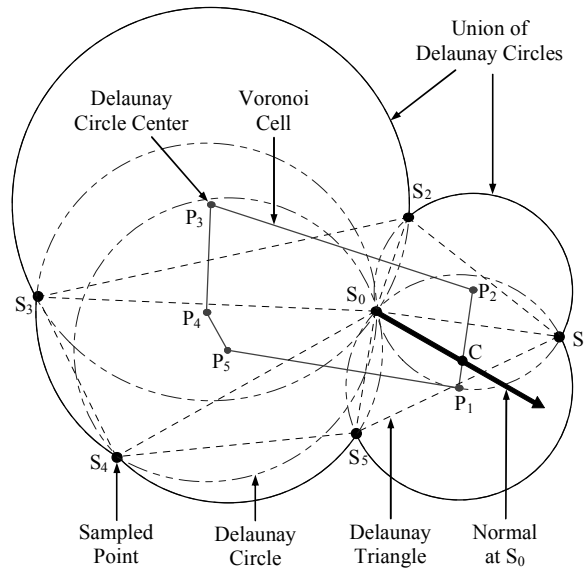

Fig. 1: Typical Voronoi diagram and Delaunay triangulation in 2D.

Suppose the normal of the sampled point $\mathbf{S}_0$ is $\mathbf{n}$, $\mathbf{S}_i$ is a Voronoi neighbor of $\mathbf{S}_0$ on the machining side, and a candidate sphere (with radius R_i and center $\mathbf{C}_i$ on $\mathbf{n}$) passes through $\mathbf{S}_0$ and $\mathbf{S}_i$:

$$\mathbf{C}_i = \mathbf{S}_0 + R_i\,\mathbf{n}$$
$$\left\| \mathbf{C}_i \mathbf{S}_i \right\| = R_i \tag{3.1}$$

The sphere radius R_i can be easily calculated for each Voronoi neighbor on the machining side of the tangent plane at $\mathbf{S}_0$. The sphere with the smallest radius is then taken as the approximated medial axis sphere at $\mathbf{S}_0$ and the corresponding $\mathbf{S}_i$ is regarded as an approximation of the global gouging point. It is evident that the approximated medial axis sphere will converge to the theoretical medial axis sphere as the sampled point density increases. It should be noted that the above procedure is equivalent to the calculation of the intersection point $\mathbf{C}$ of $\mathbf{n}$ with the Voronoi cell of $\mathbf{S}_0$ in Fig. 1.

The computational complexity of the above algorithm to approximate the medial axis sphere is $\mathbf{O}(kn)$, where k is the expected number of Voronoi neighbors for each sampled point. Since the complexity of Voronoi diagram computation is $\mathbf{O}(n \log n)$, the overall computational complexity is $\mathbf{O}(n \log n)$. The presented algorithm is thus much more efficient than the existing method which searches every sampled point in the data set and has complexity $\mathbf{O}(n^2)$ as indicated previously.

4. PRELIMINARY EVALUATION

In order to illustrate the properties of the approximated medial axis spheres generated in this work, point cloud data were obtained from several NURBS surfaces. These data sets were sampled from the parametric expressions $\mathbf{P}(u,v)$ of the surfaces at predefined intervals of the two independent parameters u and v according to the desired sampling density. Each point's surface normal was also recorded when it was sampled. Fig. 2 shows three typical point cloud data sets used in this work. It can be seen that the surface of Fig. 2(c) is more geometrically complex than that of Fig. 2(b), which is again more complex than that of Fig. 2(a).

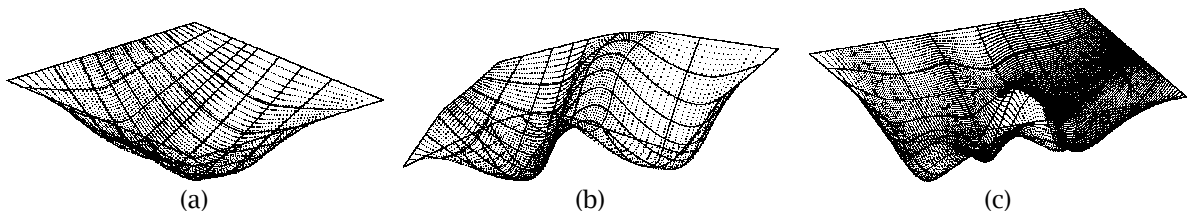| (a) | (b) | (c) |

Fig. 2: Typical point cloud data sets used in the present work.

After the Voronoi diagram and Delaunay triangulation computation of such a point cloud data set, each point was associated with one Delaunay pole sphere and one approximated medial axis sphere on the machining side of the sampled surface. The Delaunay pole sphere at a sampled point was defined as the largest Delaunay sphere incident to the point on the machining side of the surface [1],[15]. Since the surface normal of every sampled point was known, the Delaunay pole sphere at the point was identified as the largest Delaunay sphere among the incident Delaunay spheres whose centers were located on the machining side of the point's tangent plane. The approximated medial axis sphere for a sampled point was calculated using the algorithm introduced in the previous section. Thus for each valid sampled point a direct comparison between the two spheres can be made. A valid point is one for which the Delaunay pole sphere and the medial axis sphere are of finite size. It should be pointed out that any sampled point on the convex hull of the point cloud data set cannot be a valid point as its Delaunay pole sphere and medial axis sphere are both unobtainable/undefined on the outward (machining) side of the sampled surface.

It is evident that the Delaunay pole sphere is invariably larger than its corresponding medial axis sphere due to the fact that it not only must touch the point of interest, but also must grow to touch three other points in order to constrain its size. The medial axis sphere, however, grows in the direction of the surface normal and only touches one other point, resulting in a sphere that is always smaller. The Delaunay pole sphere's perimeter is forced to grow and extend in-between the points it touches, and hence very likely gouges the surface in those areas. Nonetheless, it is proven that the Delaunay pole sphere will converge to the theoretical medial axis sphere as point density increases [1].

Since both the Delaunay pole sphere and the approximated medial axis sphere will converge to the theoretical medial axis sphere as point density increases, and it is in general difficult to construct the exact medial axis in the 3D space, comparison of the applicability of the two spheres was made according to the consistency in the calculated results at reduced point densities. In this work, the Delaunay pole sphere and the approximated medial axis sphere at a given point in a highly dense sampled point cloud data set was evaluated first and regarded as the reference. These two spheres'

diameters are denoted as D_{DP0} and D_{MA0}, respectively. Reduced point density was achieved by randomly deleting 10 to 90% of points from the original data set. The two spheres, with diameters respectively denoted as D_{DPr} and D_{MAr}, were calculated again at each point in the reduced data sets. It is evident that D_{DP0} is always smaller than D_{DPr} and D_{MA0} is always smaller than D_{MAr} since the reduced data sets are always subsets of the original data.

The deviation between the Delaunay pole spheres for the original and reduced data sets at a sampled point was quantified as:

$$\delta_{DPr} = \frac{D_{DPr} - D_{DP0}}{D_{DP0}} \times 100\%$$
(4.1)

Similarly, the deviation between the approximated medial axis spheres was quantified as:

$$\delta_{MAr} = \frac{D_{MAr} - D_{MA0}}{D_{MA0}} \times 100\%$$
(4.2)

Comparisons of the average deviations and the corresponding root mean square (RMS) values of the deviations for the three point cloud data sets (Fig. 2) are shown in Figs. 3-5. It can be seen that the approximated medial axis sphere yields much smaller deviations and better consistency than the Delaunay pole sphere.
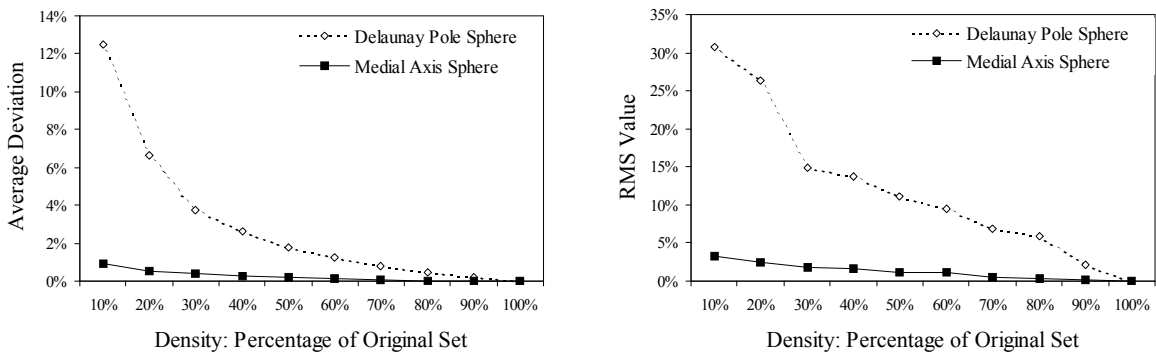

Fig. 3: Consistency comparison of Delaunay pole spheres and approximated medial axis spheres with reduced point densities for the data set of Fig. 2(a).
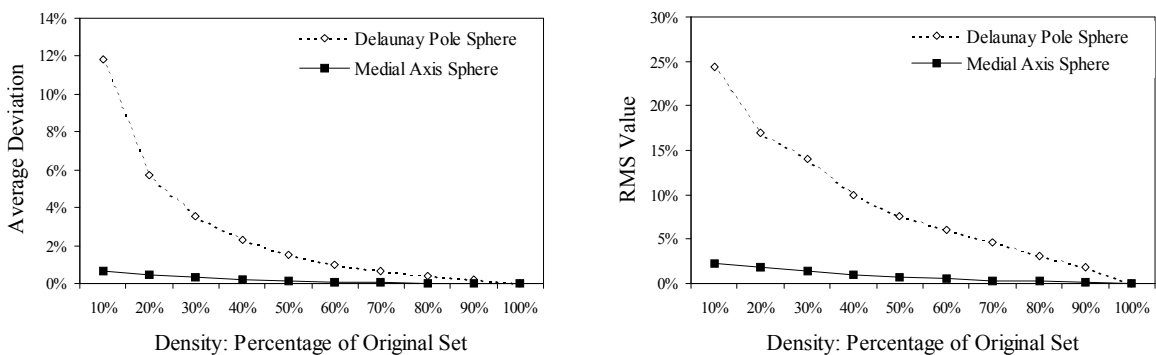

Fig. 4: Consistency comparison of Delaunay pole spheres and approximated medial axis spheres with reduced point densities for the data set of Fig. 2(b).

It is clear from the figures that the point density of a data set has a dominating effect on the accuracy of the calculated results due to the resolution of the surface representation. Also evident are the high deviations of Delaunay pole spheres when the surfaces are represented by low-density points. The deviations are particularly pronounced because Delaunay pole spheres are able to grow larger and shift the location of their centers in surface regions with high curvature and low point density. This is a direct result of the inter-point spacing, not necessarily the linear distance between the sampled points, but the true distance along the surface if it were there [15]. The Delaunay pole sphere is able to grow in-between the sampled points when the true surface geometry is unknown. And it is from here that the errors stem.
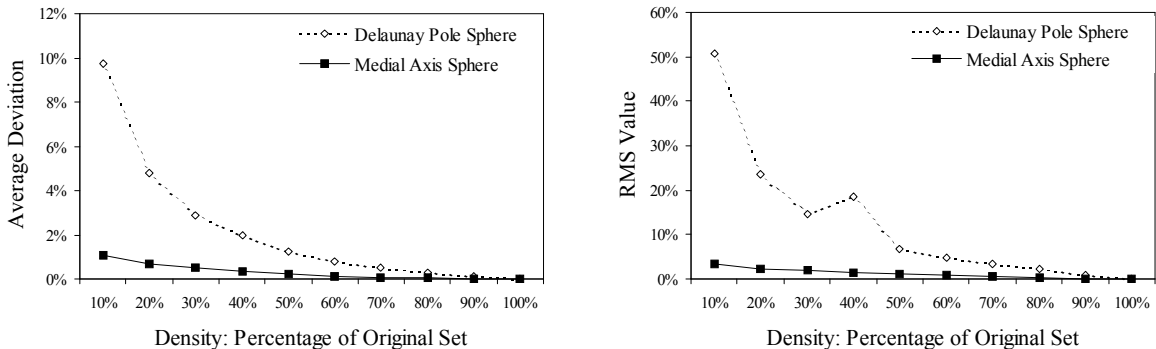

Fig. 5: Consistency comparison of Delaunay pole spheres and approximated medial axis spheres with reduced point densities for the data set of Fig. 2(c).

5. IMPROVEMENT OF APPROXIMATION ACCURACY

5.1 Surfaces of Known Geometry

As stated above, the point density of a data set has a dominating effect on the accuracy of the approximation results. When the point density increases, the computational time would increase quite dramatically as the computational complexity is $\mathbf{O}(n \log n)$. To improve the approximation accuracy of the medial axis sphere at a sampled point while keeping the number of points the same for calculating and constructing the Voronoi diagram (and not repeatably reconstructing the Voronoi diagram), it is proposed that more points be sampled and evaluated in the vicinity of the Voronoi neighbors of the sampled point, to see if a better representative of the global gouging point can be identified.

To demonstrate the improvement, for each surface shown in Fig. 2, two sampled point data sets, PS1 and PS2, were obtained from the parametric expression $\mathbf{P}(u,v)$: PS1 was sampled in the parametric space at intervals $\Delta u_1 = 0.01$ and $\Delta v_1 = 0.005$ and PS2 was sampled at intervals $\Delta u_2 = 2\Delta u_1 = 0.02$ and $\Delta v_2 = 2\Delta v_1 = 0.01$. In other words, PS2 was a subset of PS1, with one quarter the number of points. The approximated medial axis sphere at each point in PS1 and PS2 was evaluated first using the standard method presented in Section 3 with the result of PS1 regarded as the reference. The calculated diameters are denoted as D_{REF} and D_{STD}, respectively, for the same point in PS1 and PS2. The improved medial axis sphere at each point in the reduced data set PS2 was obtained via:

For each point in PS2, calculate the medial axis sphere size using Eqn. (3.1) for every incident Voronoi neighbor identified in PS2 as well as the corresponding locally added sampled points from PS1. The sphere with the smallest diameter was taken as the approximated medial axis sphere at the point. The diameter is denoted as D_{IMP}.

Similar to Eqns. (4.1) and (4.2), the error of the approximated medial axis spheres in PS2 using the standard method (with PS1 results regarded as the reference) can be quantified as:

$$\varepsilon_{STD} = \frac{D_{STD} - D_{REF}}{D_{REF}} \times 100\% \tag{5.1}$$

And the error of the approximated medial axis spheres in PS2 using the improved method can be quantified as:

$$\varepsilon_{IMP} = \frac{D_{IMP} - D_{REF}}{D_{REF}} \times 100\% \tag{5.2}$$

Comparisons of the average errors and the corresponding RMS values of the errors for the three point cloud data sets (Fig. 2) are shown in Fig. 6. It can be seen that the improved method yields more accurate results than the standard method. It should be noted that in Fig. 6 the average error for the improved method is not zero although it is very close to zero. The reason is that for certain points in PS2, the identified global gouging points are not the same as those found by using PS1. In other words, for certain points in PS2, say S_i, the PS1 global gouging point is not in the local neighborhood of PS2 Voronoi neighbors of S_i. This also leads to the RMS values in Fig. 6 not being zero.
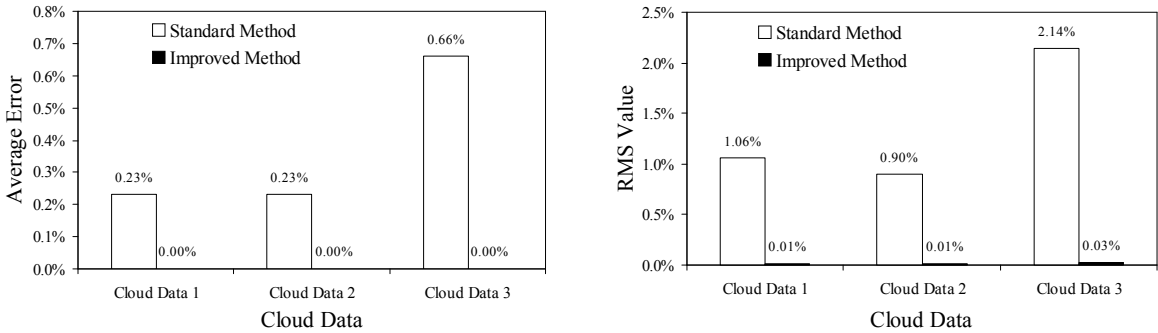

Fig. 6: Comparison of standard and improved method in approximation accuracy.

With the accuracy improvement, the benefit in computational time savings for the improved method becomes evident. Fig. 7 shows the computational time comparison for calculating the medial axis spheres with almost the same accuracy (as shown in Fig. 6). The computational time of the improved method for the 75% reduced data set is about 13% of the computational time of the standard method for the original data set.
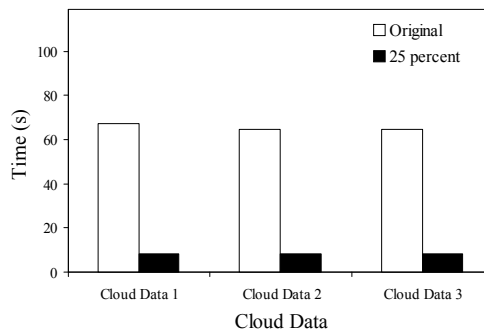

Fig. 7: Comparison of standard and improved method in computational time with the same accuracy.

5.2 Surfaces of Unknown Geometry

If the points are measured data points from a physical object surface with an unknown mathematical representation, the method developed by OuYang and Feng [14] can be used to establish the local triangular mesh surface for each point and estimate its normal vector. Thus, the method presented in Section 3 can still be used to approximate the medial axis sphere at every point. The accuracy of a point's approximated medial axis sphere can be improved by decreasing the size of the approximated sphere to avoid intersecting the local triangular mesh facets of any of its global Voronoi neighbors (not including the local Voronoi neighbors). This accuracy improvement method can be demonstrated clearly for 2D cases. In the 2D space, the approximated medial axis corresponds to the trajectory of the center of the medial axis circle at each point. Fig. 8 shows the curve reconstruction result for the Sharp Star point cloud data set [7]. Each point's normal vector was estimated as the normal vector on the fitted quadric curve of the point and its two immediate (connected) neighbors. The medial axis circle at each point was first generated by using the standard method presented in Section 3, and then it was reduced along its estimated normal vector to avoid intersecting the line segments incident to its global Voronoi neighbors.
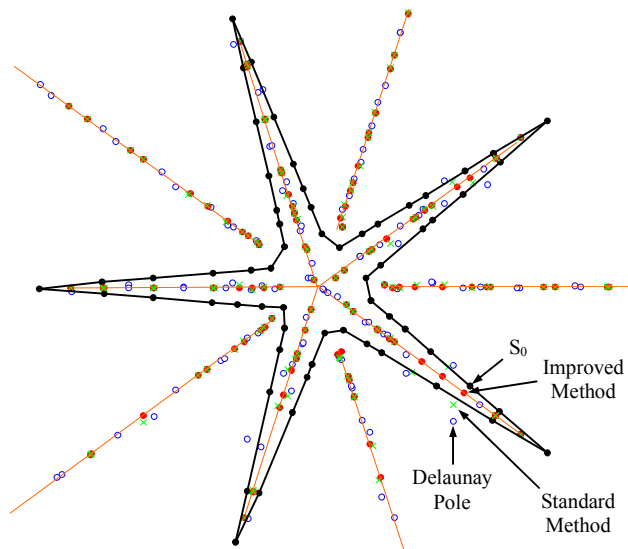

Fig. 8: Medial axis approximation for the Sharp Star data set.

Fig. 9 illustrates the improved accuracy for the point S_0 in Fig. 8, for which the standard method offers the worst approximation accuracy. In this figure, S_1 and S_4 are the local Voronoi neighbors of S_0, S_2 and S_3 are two global Voronoi neighbors of S_0 and P_1, P_2 and P_3 are three related Voronoi vertices of S_0. Note that P_2 is the Delaunay pole sphere center for S_0. The medial axis circle approximated by the standard method presented in Section 3 passes through S_0 and S_3, and its center lies on the approximated normal vector. It can be seen from Fig. 9 that this circle intersects the segment S_2S_3, which is incident to both S_2 and S_3, two global Voronoi neighbors of S_0. This circle is thus reduced along the estimated normal vector to avoid intersecting the line segment S_2S_3 to establish the resulting improved medial axis circle. It should be emphasized that the improved medial axis circle may intersect the line segments S_0S_1 and S_0S_4, which are incident to the local Voronoi neighbors of S_0, but not incident to any global Voronoi neighbor of S_0. In Fig. 8, the estimated medial axis circle centers

obtained via the proposed standard and improved method are shown. It can be seen that all Delaunay poles and approximated medial axis circle centers by the standard method as well as their improved solutions are all close to the theoretical medial axis. However, the deviations for the Delaunay poles are apparently much larger than those for the approximated medial axis circle centers, with the center positions established by the improved method being the most accurate.
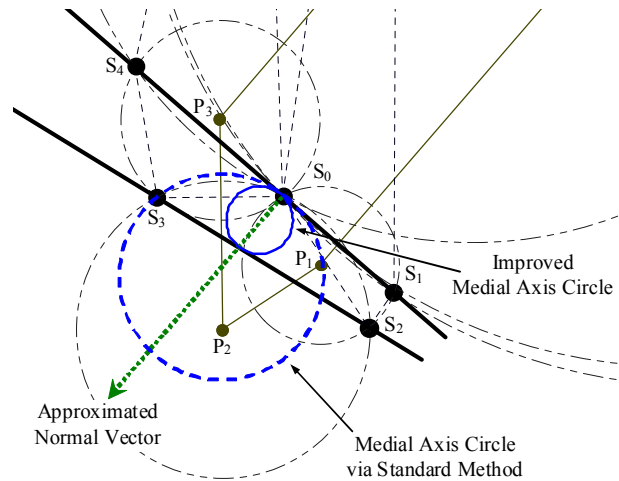

Fig. 9: Improved medial axis circle approximation for $\mathbf{S}_0$ in Fig. 8.

6. CONCLUSIONS

Optimal cutting tool selection is an active research subject in computer-aided machining process planning. A larger cutter leads to many machining benefits such as higher machining rigidity and feed rate than a smaller cutter. The major constraint is geometry-oriented due to the possible tool gouging or interference with the desired part surface with its increased size. Presented in this work are effective methods for the approximation of medial axis spheres for discrete coordinate points, which are either sampled from surfaces of known geometry or measured from surfaces of unknown geometry. Since the medial axis sphere at each point is a global geometric property and equivalent to the determination of the associated gouge-free ball-end mill, the proposed methods can be directly applied to selecting the optimal size of ball-end mills in the three-axis machining of free-form surface geometry. A more complicated tool access problem arises in five-axis free-form surface machining where the tool would be subject to interference with the work part at the tool shank due to the changing orientation of the tool. Determining the largest possible tool size in five-axis machining is much more challenging than in three-axis machining and needs to consider the tool path trajectory as well as the tool orientation at each cutter contact point. The long-term objective is to fully implement the automatic tool selection module within a futuristic virtual machining simulation system.

The Voronoi diagram and Delaunay triangulation have been used to establish the global geometric relationships among the data points and to create the Delaunay pole sphere at each data point on the machining side of the surface. Centers of the Delaunay pole spheres were known to converge to the theoretical medial axis with increasing point density. If the sampled surfaces are of known geometry, approximated medial axis spheres with superior accuracy for each sampled point can be obtained efficiently by employing the point's normal vector and the local surface patches around its Voronoi neighbors. If the sampled surfaces are of unknown geometry, approximated medial axis spheres with improved accuracy for each data point can also be obtained by using the estimated normal vector at the point and the associated local triangular meshes of its global Voronoi neighbors. The correlation between the approximation accuracy and the sampled point density is, however, not explicitly known. This is an unresolved research subject and would be pursued actively.

7. ACKNOWLEDGEMENTS

8. REFERENCES

[1]   Amenta, N.; Choi, S.; Kolluri, K. R.: The power crust, unions of balls, and the medial axis transform, Computational Geometry: Theory and Applications, 19(2-3), 2001, 127-153.
[2]   Attali, D.; Montanvert, A.: Computing and simplifying 2D and 3D continuous skeletons, Computer Vision and Image Understanding, 67(3), 1997, 261-273.
[3]   Blum, H.: A transformation for extracting new descriptors of shape, Models for the Perception of Speech and Visual Form, editor: W. Wathen-Dunn, MIT Press, 1967, 362-380.
[4]   Bonnassie, A.; Peyrin, F.; Attali, D.: A new method for analyzing local shape in three-dimensional images based on medial axis transformation, IEEE Transactions on Systems, Man, and Cybernetics – Part B: Cybernetics, 33(4), 2003, 700-705.
[5]   Chuang, C. M.; Chen, C. Y.; Yau, H. T.: A reverse engineering approach to generating interference-free tool-paths in three-axis machining from scanned data of physical models, International Journal of Advanced Manufacturing Technology, 19(1), 2002, 23-31.
[6]   Culver, T.; Keyser, J.; Manocha, D.: Accurate computation of the medial axis of a polyhedron, Proceedings of the 5th ACM Symposium on Solid Modeling and Applications, 1999, 179-190.
[7]   Dey, T. K.; Wenger, R.: Fast reconstruction of curves with sharp corners, International Journal of Computational Geometry & Applications, 12(5), 2002, 353-400.
[8]   Dey, T. K.; Zhao, W.: Approximate medial axis as a Voronoi subcomplex, Computer-Aided Design, 36(2), 2004, 195-202.
[9]   Feng, H. Y.; Teng, Z.: Iso-planar piecewise linear NC tool path generation from discrete measured data points, Computer-Aided Design, 37(1), 2005, 55-64.
[10]   Kettner, L.; Näher, S.: Two computational geometry libraries: LEDA and CGAL, Handbook of Discrete and Computational Geometry, 2nd ed., editors: J. E. Goodman and J. O'Rourke, Chapman & Hall, Boca Raton, 2004, 1435-1463.
[11]   Lee, Y. S.; Choi, B. K.; Chang, T. C.: Cut distribution and cutter selection for sculptured surface cavity machining, International Journal of Production Research, 30(6), 1993, 1447-1470.
[12]   Lim, T.; Corney, J.; Clark, D. E. R.: Exact tool sizing for feature accessibility, International Journal of Advanced Manufacturing Technology, 16(11), 2000, 791-802.
[13]   Lin, A. C.; Liu, H. T.: Automatic generation of NC cutter path from massive data points, Computer-Aided Design, 30(1), 1998, 77-90.
[14]   OuYang, D.; Feng, H. Y.: On the normal vector estimation for point cloud data from smooth surfaces, Computer-Aided Design, 37(10), 2005, 1071-1079.
[15]   OuYang, D.; Van Nest, B. A.; Feng, H. Y.: Determining gouge-free ball-end mills for 3D surface machining from point cloud data, Robotics and Computer-Integrated Manufacturing, 21(4-5), 2005, 338-345.
[16]   OuYang, D.; Feng, H. Y.: Machining triangular mesh surfaces via mesh offset based tool paths, Computer-Aided Design and Applications, 5(1-4), 2008, 254-265.
[17]   Park, S. C.; Chung, Y. C.: Tool-path generation from measured data, Computer-Aided Design, 35(5), 2003, 467-475.
[18]   Ranjan, V.; Fournier, A.: Matching and interpolation of shapes using unions of circles, Computer Graphics Forum, 15(3), 1996, 129-142.
[19]   Sheehy, D. J.; Armstrong, C. G.; Robinson, D. J.: Shape description by medial surface construction, IEEE Transactions on Visualization and Computer Graphics, 2(1), 1996, 62-72.
[20]   Sherbrooke, E. C.; Patrikalakis, N. M.; Brisson, E.: An algorithm for the medial axis transform of 3D polyhedral solids, IEEE Transactions on Visualization and Computer Graphics, 2(1), 1996, 44-61.
[21]   Veeramani, D.; Gau, Y. S.: Selection of an optimal set of cutting tool sizes for 2.5D pocket machining, Computer-Aided Design, 29(12), 1997, 869-877.
[22]   Yao, Z.; Gupta, S. K.; Nau, D. S.: Algorithms for selecting cutters in multi-part milling problems, Computer-Aided Design, 35(9), 2003, 825-839.